Intermediate Species Profiles in Low-Pressure Methane/Oxygen Flames Inhibited by 2-H Heptafluoropropane: Comparison of Experimental Data with Kinetic Modeling

BRADLEY A. WILLIAMS*, DREW M. L' ESPÉRANCE, AND JAMES W. FLEMING

Chemistry Division, Naval Research Laboratory, Washington, DC 20375-5342

Experimental profiles of the intermediate species H, OH, CH, CF, CF_2, and CHF are obtained in a 10 torr premixed flat flame of methane/oxygen in a 1:2 molar ratio, inhibited by a 4% mole fraction of 2-H heptafluoropropane (HFP, CF_3CHFCF_3). These data are compared to calculations using a recently published kinetic mechanism describing the consumption of this fire suppression agent. The profiles in the flame inhibited by HFP are compared to previously published data for flames containing CHF_3 and CH_2F_2 under the same conditions of stoichiometry and flux of fluorine atoms. The species profiles relative to the flames containing the fluoromethanes are accurately predicted and atmospheric pressure flame speeds are fairly well predicted by the kinetic mechanism. Under equal fluorine loadings, profiles of temperature and of H and OH mole fraction are virtually identical between the flames containing HFP and CHF_3. The flame inhibited by HFP, however, has approximately twice as much CH* emission as the flame containing CHF_3. The kinetic model predicts that thermal decomposition, rather than H atom abstraction, is the primary destruction mechanism for HFP under the conditions studied. © 1999 by The Combustion Institute

INTRODUCTION

2-H heptafluoropropane (commonly referred to as HFP or HFC-227ea, having the chemical structure CF_3CHFCF_3) is coming into widespread use as a fire suppressant [1] to replace brominated compounds such as Halon 1301 (CF_3Br), whose production has been prohibited in developed countries by international treaty. Due to the practical importance of HFP in fire protection, as well as its somewhat lower suppression efficiency than Halon 1301 [2, 3], it is desirable to understand this compound's chemical behavior in flame environments. Of particular importance is the origin and magnitude of suppression due to fluorine chemistry, as opposed to physical effects of the agent's addition to the flame.

A kinetic mechanism for combustion chemistry of C_1 and C_2 fluorocarbons has been developed at the U.S. National Institute of Standards and Technology (NIST) [4–6]. Recently, our laboratory has published profiles of several intermediate species in premixed low-pressure methane/oxygen flames containing the series of fluoromethanes [7]. These experimental data were compared to predictions of the NIST fluorocarbon mechanism, and some refinements to the kinetics were suggested on the basis of validation against both low-pressure species profile data and atmospheric pressure flame speed measurements.

During our experimental study of fluoromethane-inhibited low-pressure flames, we also recorded profiles in a flame inhibited by HFP. These data were not included in Ref. 7, because the fluorine kinetic mechanism did not include any C_3 compounds, and only qualitative interpretations of the flame structure could be made. More recently, Hynes et al. proposed a kinetic mechanism [8] for the initial breakdown of HFP into C_1 and C_2 fragments. When added to the NIST HFC mechanism, the HFP submechanism permits kinetic modeling of HFP-inhibited flames. In Ref. 8, kinetic model predictions were compared to experimental measurements of postflame concentrations of stable species in lean atmospheric pressure hydrogen/air flames inhibited by HFP. Hynes et al. have since published a shock tube study of HFP decomposition in a pyrolytic environment [9], and reported stable species profiles in an atmospheric pressure hydrogen/ethane/air/HFP flame [10].

---

*Corresponding author. E-mail: brad@code6185.nrl.navy.mil
National Research Council Postdoctoral Associate 1995–97.
Present address: Department of Physical Sciences, New Mexico Highlands University, Las Vegas, NM 87701-4073.

Flame Conditions

Agent	Flow Rates (cm³/min@0°C)			Adiabatic Flame Temperature (K)[a]	ϕ	Mass Flow (g/cm²-s)
	CH_4	O_2	Agent			
none	400	800	0	2571	1.00	0.86×10^{-3}
CH_2F_2	342	800	175	2557	1.07	1.08×10^{-3}
CHF_3	400	800	117	2548	1.07	1.08×10^{-3}
C_3HF_7	400	800	50	2560	1.08	1.09×10^{-3}

Profiles of several stable and intermediate species in low-pressure methane/oxygen/argon flames inhibited by HFP were presented by Battin-Leclerc et al., in Ref. 1. The profiles were compared to those of an uninhibited flame, and a flame inhibited by C_2F_6. The experimental flame structure gave reasonable agreement with predictions of a kinetic model taken from the work of Westbrook [11] on inhibition by CF_3Br, with some additional steps added to account for the initial breakdown of the inhibitor into C_1 fluorinated species. In the present study we use the NIST kinetic mechanism as a starting point, since it is more comprehensive than the mechanism of Westbrook especially in terms of C_2 chemistry. Hynes et al. developed their HFP submechanism using the NIST mechanism to describe the C_1 and C_2 fluorocarbon kinetics.

Here we compare the predictions of the HFP kinetic mechanism (the C_3 submechanism of Hynes et al. [8–10] added to the HFC mechanism revised according to Ref. 7), with experimental species profiles. The flame conditions of our study are quite different from those in Ref. 8, having considerably higher peak temperatures, slightly rich stoichiometry, and hydrocarbon fuel, as well as being at reduced pressure. We validate the combined mechanism against the atmospheric pressure flame speed data of Linteris et al. [12], who investigated premixed methane/air flames inhibited by several fluoroethanes and fluoropropanes, including HFP. Kinetic modeling predictions of adiabatic flame speeds were reported in Ref. 12 for the mixtures containing fluoroethanes but not fluoropropanes. We compare modeling predictions of the present mechanism with those of Hynes et al. presented in Ref. 10. Based on comparison of the model predictions to the experimental data sets, we suggest some refinements to the C_2 chemistry in the NIST HFC mechanism.

EXPERIMENTAL

The experimental apparatus and procedures were identical to those used in our study on flames containing fluoromethanes [7]. The HFP-inhibited flame maintained at 10 torr consisted of a stoichiometric methane/oxygen mixture with 4% mole fraction of HPF added. This flame contained an equal number of fluorine atoms as the flame inhibited by 8.9% mole fraction of trifluoromethane, the standard condition for this agent used in Ref. 7. The overall equivalence ratio (taking into account the agent) was also nearly identical, $\phi = 1.08$ compared to 1.07 for the flame containing 8.9% CHF_3. Flow conditions of the HFP-inhibited flame, as well as the uninhibited flame and flames inhibited by CHF_3 and CH_2F_2 used for comparison of intermediate species profiles, are listed in Table 1.

The flame species H, OH, CH, CF, CHF, and CF_2 were monitored by laser-induced fluorescence; the detection schemes for these species are listed in Table 2, and have been more completely described previously [7, 13]. Flame temperature profiles were determined from laser-induced fluorescence (LIF) spectra of the OH radical. Profiles of CH* chemiluminescence at 430 nm were also recorded. All species profiles were measured on a relative basis. Profiles from an appropriate reference flame (uninhibited, CHF_3-inhibited, or CH_2F_2-inhibited) were recorded in immediate succession to those in the flame inhibited by HFP, so that the relative concentrations of the radical species for the different flame conditions can be directly compared. The structure and chemistry of the flames inhibited by fluoromethanes is discussed elsewhere [7]; the present study is focused on the structure of the HFP-inhibited flame in

TABLE 2

Optical Diagnostics Used for Detection of Flame Species

Species	Transition	Excitation Wavelength (nm)	Excitation Energy (μJ)	Emission Wavelength (nm)
H	1s-2s–4p (3 photon)	243.1(2-photon) +486.1	150 10	486
OH	R_1(8)A–X (1,0)	281.27	30	311
CH	Q_1(6)B–X(0,0)	389.98	200	390
CF	Q_2(21.5) + P_1(26.5)+ Q_1(19.5)A–A(1,0)	223.30	200	255 ± 15
CF_2	A–X	250	60	334 ± 20
CHF	A–X(0,3,0)-(0,0,0)	492.42	300	>515 nm

comparison to those containing the C_1 compounds.

LIF profiles were obtained by correcting the measured LIF signal for changes in the intensity of the laser used to excite fluorescence. The corrected LIF profiles have been converted to species mole fraction by correcting for gas density changes and the temperature dependence of the ro-vibronic level probed. For the species CHF the correction is very uncertain because the rotational structure has not been completely analyzed, and interference is present in the region between 5–10 mm above the burner.
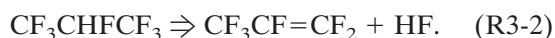
The LIF signals have not been corrected for quenching variations between flames. The fluorescence signal was integrated over an interval of approximately 20 ns immediately following the laser pulse to minimize the influence of quenching. For most species probed, fluorescence lifetimes were on the order of 150–200 ns for all flame conditions. The only exceptions are CF and CF_2, which have short fluorescence lifetimes (<50 ns) due to radiative decay and predissociation, and hence are relatively unaffected by quenching. We estimate the experimental uncertainties in the ratios of LIF signals between different flames to be $\pm 10\%$.

KINETIC MECHANISM AND MODELING

The chemical structures of the inhibited flames were modeled using the Sandia PREMIX and related codes [14–16]. The kinetic mechanism and thermodynamic database used for the H/C/O chemistry for one-carbon and two-carbon species was the Gas Research Institute

GRI-Mech 2.11 [17], with nitrogen chemistry deleted. The NIST HFC mechanism, as refined in Ref. 7, was used for the thermodynamics and reactions of the C_1 and C_2 fluorinated species. This mechanism gave good agreement with both flame speed measurements and species profiles of methane flames containing fluoromethanes [7]. For the initial breakdown of HFP, the reaction set from Ref. 8 was used as the starting point.

This mechanism detailed above was modified in the following ways (Table 3). First, the original NIST HFC mechanism did not include reactions of the CF_3-CHF radical (a major thermal decomposition product of HFP) with atomic hydrogen. In Ref. 12 kinetics for two product channels of this reaction were proposed, as were revised kinetics for a few other reactions. We adopted four of the reactions proposed in Ref. 12, including the two CF_3-CHF + H reactions. The rate expressions from Ref. 9 were used for the HFP thermal decomposition reactions (numbers refer to Table 3)

$$CF_3CHFCF_3 \Rightarrow CF_3CHF + CF_3, \qquad \text{(R3-1)}$$

$$CF_3CHFCF_3 \Rightarrow CF_3CF{=}CF_2 + HF. \quad \text{(R3-2)}$$

Thermal decomposition for CF_3CHF,

$$CF_3CHF \Rightarrow CF_2{=}CHF + F, \qquad \text{(R3-19)}$$

was added to the mechanism, with parameters from Ref. 9. Additional reactions suggested by Hynes et al. [10, 18] for HFP and products (mostly reactions with hydrocarbon radicals) have been added to the reaction set. Finally, additional product channels (discussed in more detail below) were added for the reactions of O and OH with $CF_2{=}CHF$.

TABLE 3

Kinetic Mechanism

Mechanism consists of GRI-Mech 2.11, NIST HFC mechanism as revised in Ref. [7], HFP submechanism of Ref. [8], with the following changes:

Reaction	Arrhenius Parameters $k(T) = AT^b\exp(-E_a/RT)$			
	A(mol, cm, s)	b	E_a (cal/mol)	Ref.
1. $C_3F_7H(+M) = CF_3 + CF_3-CHF(+M)$				
high-pressure limit	7.9E + 15	0.0	85,000	[9]
low-pressure limit	3.46E + 21	0.0	85,000	a,b
2. $C_3F_7H(+M) = C_3F_6 + HF(+M)$				
high-pressure limit	7.9E + 12	0.0	69,600	[9]
low-pressure limit	3.46E + 18	0.0	69,600	a,b
3. $C_3F_7H + CH_3 = C_3F_7CH_4$	5.7E + 10	0.0	9,500	[10]
4. $C_3F_7H + C_2H_3 = C_3F_7 + C_2H_4$	6.0E + 10	0.0	7,000	[18]
5. $C_3F_7(+M) = CF_2{:}CF_2CF_3(+M)$				
high-pressure limit	1.0E + 14	0.0	76,000	[8]
low-pressure limit	4.38E + 19	0.0	76,000	a,b
6. $C_3F_7(+M) = C_3F_6 + F(+M)$				
high-pressure limit	2.0E + 14	0.0	69,000	[8]
low-pressure limit	8.75E + 19	0.0	69,000	a,b
7. $CF_3-CHF + CF_3 = C_3F_6 + HF$	7.0E + 16	−1.17	4,330	[18]
8. $C_3F_6 + O = CF_3COF + CF_2$	5.8E + 12	0.0	2,500	[10]
9. $C_3F_6(+M) = CF_3 + CF_2{:}CF(+M)$				
high-pressure limit	3.2E + 13	0.0	105,600	[8]
low-pressure limit	1.4E + 19	0.0	105,600	a,b
10. $C_3F_6(+M) = CF_2{:}CF_2 + CF_2(+M)$				
high-pressure limit	3.2E + 13	0.0	94,000	[8]
low-pressure limit	1.4E + 19	0.0	94,000	a,b
11. $CF_3CHO + CH_3 = CF_3CO + CH_4$	1.0E + 11	0.0	7,400	[18]
12. $CF_3CHO(+M) = CF_2CO + HF(+M)$				
high-pressure limit	1.0E + 13	0.0	30,000	[8]
low-pressure limit	8.75E + 18	0.0	30,000	a,b
13. $CF_3CHO(+M) = CF_3 + HCO(+M)$				
high-pressure limit	4.0E + 16	0.0	80,000	[8]
low-pressure limit	3.5E + 21	0.0	80,000	a,b
14. $CF_3COF(+M) = CF_3 + CF{:}O(+M)$				
high-pressure limit	4.3E + 16	0.0	90,000	[8]
low-pressure limit	3.76E + 21	0.0	90,000	a,b
15. $CF{:}O + CHF_2 = CF_2CO + HF$	2.7E + 13	0.0	20,000	[12]
16. $CF3-CHF + H = CHF{:}CF_2 + HF$	6.56E + 24	−3.57	4,225	[12]
17. $CF3-CHF + H = CH2F + CF3$	4.28E + 16	−0.74	4,750	[12]
18. $HCO + CF_3 = CF_2CO + HF$	2.7E + 13	0.0	0	[12]
19. $CF_3-CHF(+M) = CHF{:}CF_2 + F(+M)$				
high-pressure limit	6.3E + 14	0.0	62,000	[9]
low-pressure limit	5.51E + 19	0.0	62,000	a,b
20. $CHF{:}CF_2 + O = CF_2 + CHF{:}O$	3.21E + 06	2.0	0	a
21. $CHF{:}CF_2 + O = CHF + CF_2{:}O$	3.2E + 06	2.0	2,000	a
22. $CHF{:}CF_2 + OH = CF_2{:}O + CH_2F$	2.0E + 06	2.0	2,850	a
23. $CHF{:}CF_2 + OH = CHF{:}O + CHF_2$	4.0E + 06	2.0	2,850	a

[a] Estimated, see text.

[b] Third-body efficiencies: H_2O:9.0, CH_4:2.0, CO:1.5, CO_2:2.0, C_2H_6:3.0, CH_3F:6.0, CH_2F_2:6.0, CHF_3:6.0, C_3F_7H:12.0, HF:2.0.

Falloff behavior for the thermal decomposition reactions in the HFP mechanism was estimated, since low-pressure kinetic studies were not always available for analogous hydrocarbon reactions. For the low-pressure Arrhenius parameters, the activation energy was assumed to be identical to that in the high-pressure limit. The preexponential factor was chosen such that

at a temperature of 1600 K, the transition between low-pressure and high-pressure behavior occurs at 1.5 atm for C_2 species (in nitrogen) and 0.3 atm for C_3 species. Kinetics in the transition region were assumed to follow the Lindemann form. Third-body efficiencies relative to nitrogen were the same used for the fluoromethane decomposition reactions in Ref. 7. For HFP itself, a third-body efficiency of 12 was used.

Calculations of the experimental burner-stabilized flames were performed using the experimental temperature profiles as input. Multicomponent viscosities (the keyword MULT in the PREMIX code) and thermal diffusivities for H and H_2 (TDIF keyword) were used to calculate species transport. The computational domain extended from the burner surface to 5 cm. Mesh refinement tolerances (local/global variation) for the species profiles were set to 0.1 for the species concentrations (GRAD parameter in PREMIX) and to 0.25 for the concentration gradients (CURV parameter). The final grid for the uninhibited flame contained approximately 80 mesh points, while the solutions for the inhibited flames contained approximately 110 mesh points.

TEMPERATURE PROFILES

Flame temperatures were determined from rotational energy distributions of the OH radical by exciting the A-X (1,0) band near 281 nm. For the temperature measurements, the laser energy was attenuated to <1 μJ to avoid saturation. A broadband UV Filter (Corning 7-54) was used to collect fluorescence on both the (1,1) and (0,0) transitions. Spectral scans comprising typically between 10–40 spectral lines covering a broad range of rotational energies were performed at 15 points in each of the flame conditions used. Statistical uncertainties in the temperature fits ranged from 20–45 K. Burner surface temperatures were measured by an uncoated type K (Chromel–Alumel) thermocouple. For the PREMIX calculations and in conversion of LIF data to species mole fractions, flame temperature profiles were represented by the (empirical) functional form
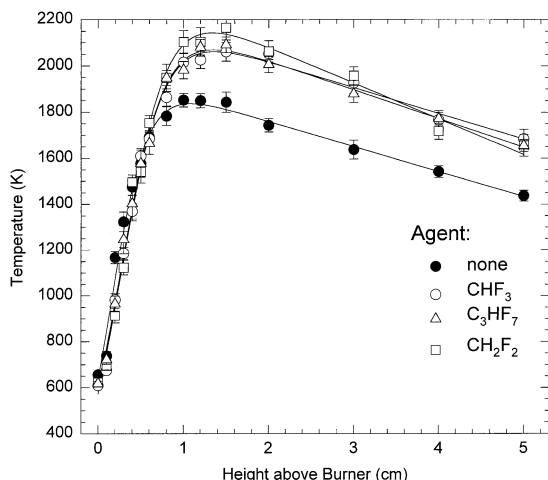

Fig. 1. Temperature profiles of the flames studied. Individual data points were determined from LIF spectra of OH; statistical uncertainties are shown. Solid lines indicate functional fits (Eq. 1) which were used as inputs to PREMIX calculations and in converting LIF profiles into relative mole fractions.

$$T(x) = \frac{A}{1 + B \exp\left(\dfrac{x - C}{D}\right)} - Ex \qquad (1)$$

where x is the height above the burner in cm. The coefficients A–E were fit to the experimental data points. The fitted functions were used as temperature inputs to the PREMIX calculations, and for converting fluorescence intensity profiles to species mole fractions.

Temperature measurements and fitted functions are shown in Fig. 1 for the HFP-inhibited flame and, for comparison, the uninhibited flame as well as the flames inhibited by CHF_3 and CH_2F_2. The temperature profile of the flame containing HFP is nearly indistinguishable from that containing trifluoromethane at an equal loading of fluorine atoms.

EMISSION PROFILES

The methane/oxygen flame becomes markedly brighter upon addition of HFP. Profiles of CH* emission at 430 nm are shown in the bottom panel of Fig. 2. The flame inhibited by HFP has twice the luminescence of the flame inhibited by CHF_3, which in turn is slightly more than three times as luminous as the uninhibited flame. In
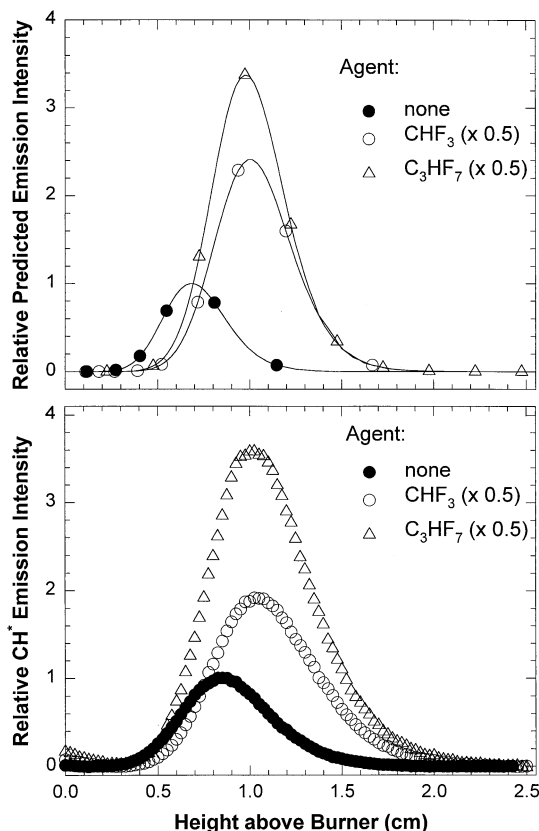
Fig. 2. CH* emission profiles (bottom) at 430 ± 10 nm for the uninhibited flame and the flames inhibited by CHF_3 and HFP. Profiles for the inhibited flames have been reduced by a factor of 2. Emission profiles (top) estimated from the PREMIX calculation by taking the product of the O atom and C_2H concentrations.

Fig. 3. Calculated (top) and measured (bottom) H atom profiles for the uninhibited flame, and the flames inhibited by CHF_3 and HFP.

the top panel of Fig. 2, CH* emission is estimated from the kinetics calculations by taking the product of the C_2H and O atom concentrations [7], since the C_2H + O reaction is thought to be primarily responsible for CH chemiluminescence. The peak value of this product compared to the uninhibited flame is quite close to the experimental ratio of the emission intensities. The kinetic model predicts that formation of C_2H in the HFP-inhibited flame occurs, as it does in flames containing fluoromethanes, through recombination of fluorinated methyl radicals with CH_3. The fact that HFP forms C_2 species in its initial decomposition steps does not account for the greater luminescence than in the CHF_3-inhibited flame. Rather, the fraction of CF_3 radicals that react with CH_3 is
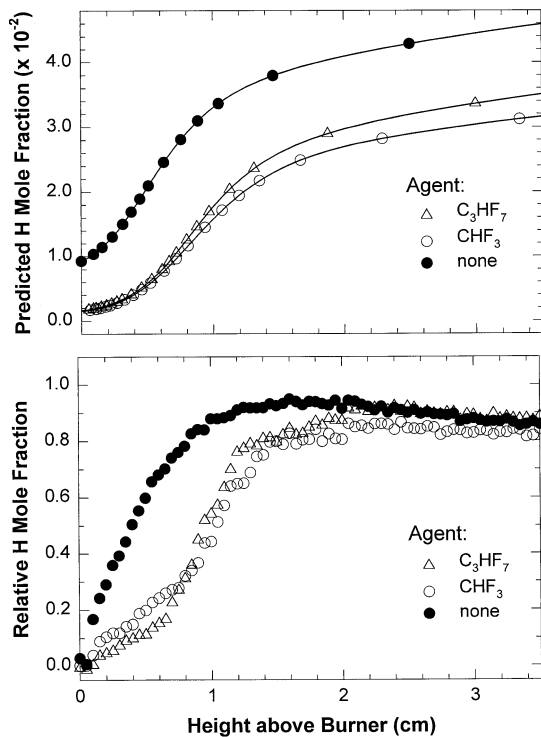
greater in the HFP flame because the agent's decomposition proceeds more quickly, leading to a better spatial overlap between the profiles of the two radicals. Also, HFP produces significant quantities of the partially fluorinated methyl radicals CH_2F and CHF_2, whose recombination with CH_3 in flames inhibited by CH_3F and CH_2F_2 leads to greater CH* chemiluminescence (at constant equivalence ratio and F:H ratio) than in the CHF_3-inhibited flame.

LIF PROFILES OF INTERMEDIATE SPECIES

Calculated and experimental profiles of H atom and OH are shown in Figs. 3 and 4, respectively. As with the temperature profile, the profiles of both these species are virtually identical between the flame inhibited by HFP and that inhibited by CHF_3 at an equal loading of fluorine atoms. The profiles of these two radicals are also nearly identical for the flames contain-
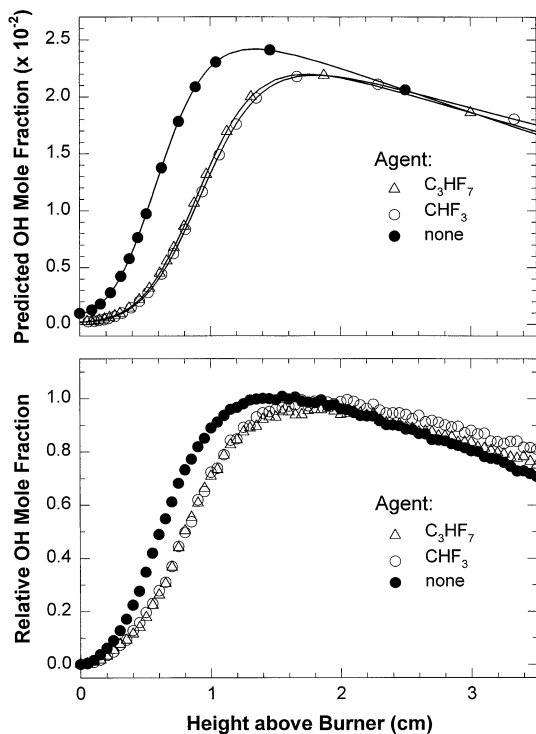
Fig. 4. Calculated (top) and measured (bottom) OH profiles for the uninhibited flame, and the flames inhibited by CHF_3 and HFP.

Fig. 5. Calculated (top) and measured (bottom) CH profiles for the uninhibited flame, and the flames inhibited by CHF_3 and HFP.

ing mono- and difluoromethane as for trifluoromethane [7]. The kinetic modeling also predicts the close similarity of the H and OH profiles between the flames inhibited by CHF_3 and HFP.

Calculated and experimental profiles of CH are shown in Fig. 5. The location of the CH mole fraction peak is nearly identical between the flames inhibited by HFP and by CHF_3, but the flame containing HFP has a slightly higher peak CH concentration. The calculation predicts that the CH peak occurs slightly earlier in the HFP-inhibited flame than in the CHF_3-inhibited flame. The CH concentrations in the two inhibited flames, both relative to each other and to the uninhibited flame, are predicted quite well by the kinetic mechanism. The additional CH predicted to be formed from HFP is produced primarily from $^1CH_2$ and CHF, which are produced in turn from CH_2F and CHF_2.

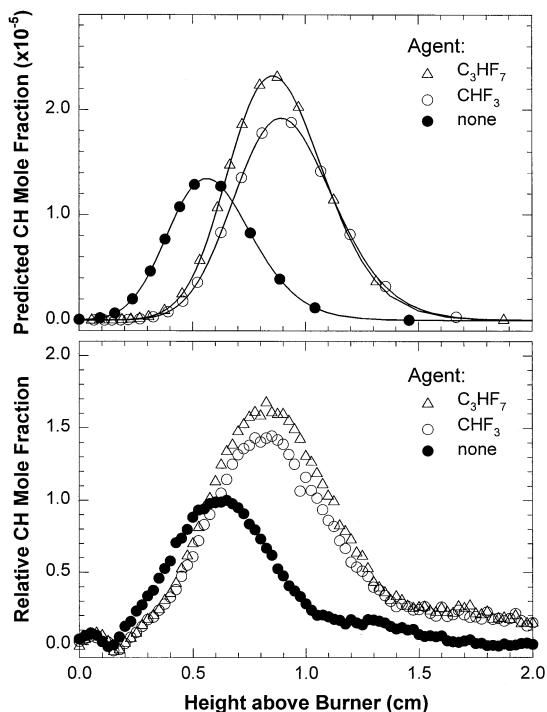Profiles of CHF are shown in Fig. 6. The CHF profile in the CH_2F_2-inhibited flame is used as a

reference for the HFP-inhibited flame, because no detectable LIF signal for this species was observed in the CHF_3-inhibited flame. The LIF profile for this species suffers from interference in the luminous zone of the flame, as well as a large and ill-defined temperature correction [7]. For these reasons, there is a great deal of uncertainty in the location of the maximum CHF concentration. The experimental data do indicate a significant production of CHF in the HFP-inhibited flame, roughly 20–30% that of the CH_2F_2-inhibited flame. The kinetic model predicts significant CHF production, in agreement with the experimental data. Analysis of the kinetic pathways (see below) indicates that CHF_2 and CH_2F are predicted to be the primary precursors to CHF.

Figures 7 and 8 show profiles of CF_2 and CF, respectively. The concentrations of these species in the HFP-inhibited flame relative to the CHF_3-inhibited flame are predicted fairly well. The CF_2 peak occurs earlier in the HFP-inhib-
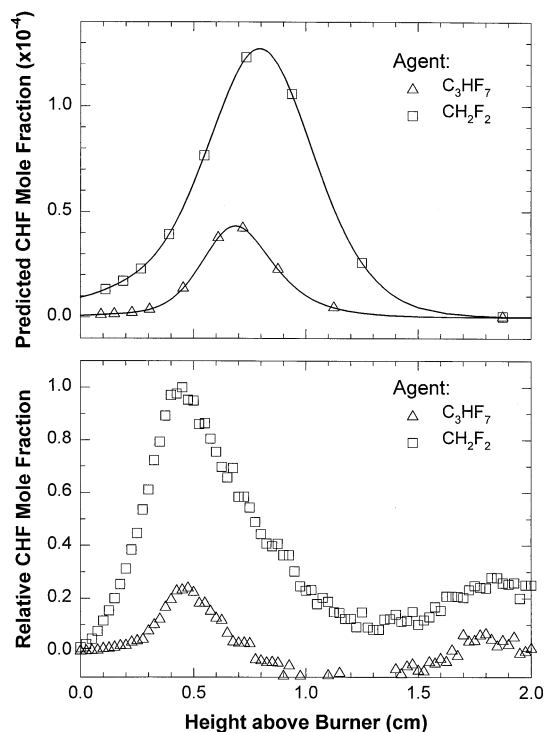
Fig. 6. Calculated (top) and measured (bottom) profiles of CHF for the flames inhibited by CH_2F_2 and HFP. The flame inhibited by CH_2F_2 was used for reference since no CHF signal was observed in the flame inhibited by CHF_3. Near 1.0 cm the profiles may have been affected by saturation of the detector due to flame emission.

Fig. 7. Calculated (top) and measured (bottom) CF_2 profiles for the flames inhibited by CHF_3 and HFP.

ited flame, which the model predicts although the profile shapes do not match exactly. The location of the CF mole fraction peak is slightly too far from the burner; this also occurs in the model prediction of all the flames inhibited by C_1 fluorocarbons.

When reaction (R19) was added to the mechanism, the peak mole fraction of CF_2 was overpredicted in the HFP-inhibited flame. Analysis of the reaction pathways indicated that CHF: CF_2 produced by (R19) should be destroyed almost exclusively by the reaction

$$CHF:CF2 + H \Rightarrow CH_2F + CF_2. \qquad (R1)$$

It is likely that attack by O and OH contribute more to this species' removal than the mechanism predicts. We added additional channels for these reactions (R3-20–R3-23), significantly improving agreement of the model with the experimental CF_2 profiles.
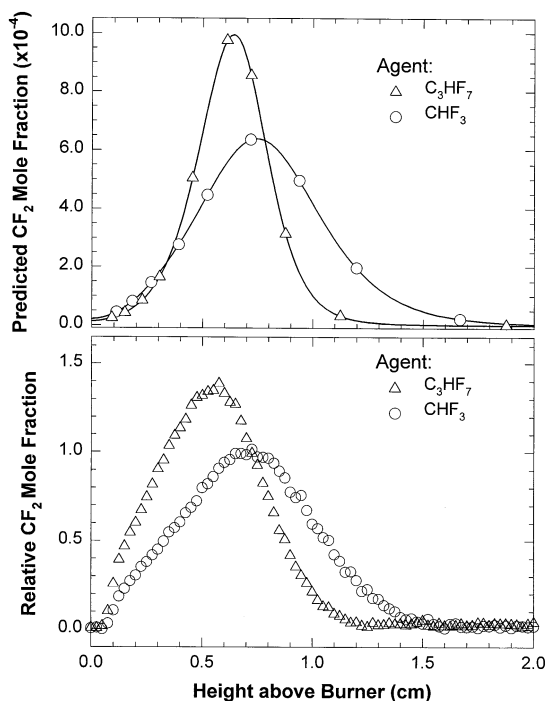
KINETIC PATHWAYS AND MECHANISM REFINEMENT

Kinetic pathways are shown in Fig. 9. Arrow thicknesses between the different fluorocarbon species are proportional to the molar flux integrated across the flame. In some cases, incoming and outgoing arrow thicknesses do not sum to zero when, for instance, a C_3 species breaks up into smaller fragments. The predicted reaction pathways in our flame conditions are considerably different than those presented by Hynes et al. in Ref. 8. In our CH_4/O_2 flames, thermal decomposition dominates agent destruction, even after falloff kinetics are added to the decomposition reactions. This is in contrast to the finding of Hynes et al., where hydrogen abstraction was predicted to account for the majority of agent destruction. The flame studied in Ref. 8 (hydrogen/air with equivalence ratios between 0.3 and 0.5) had low peak temperatures but high radical concentrations. In the present conditions, H atom abstraction from HFP (primarily by OH) accounts for only about 5% of agent destruction. We initially modeled the
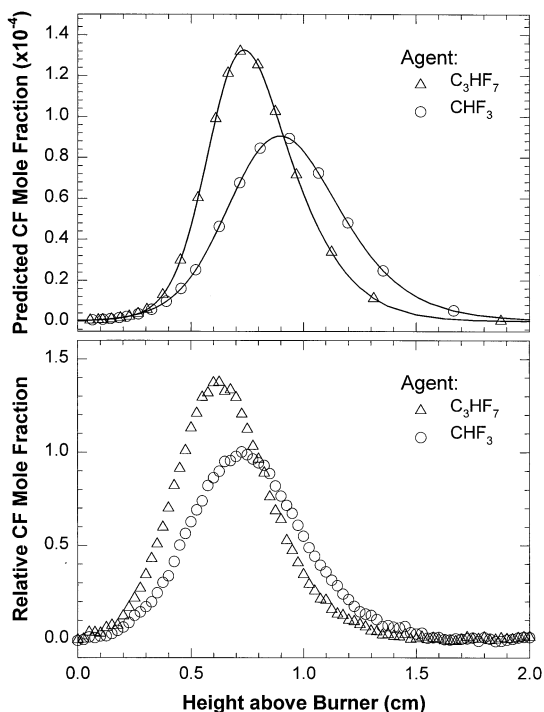
Fig. 8. Calculated (top) and measured (bottom) CF profiles for the flames inhibited by CHF_3 and HFP.
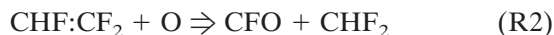
flame using the HFP mechanism of Ref. 8, which led to the prediction that HF elimination (R3-2) predominates over C-C scission (R3-1) in destroying HFP. When the kinetic expressions from Ref. 9 are used for (R3-1) and (R3-2), the calculation now shows that C-C dissociation accounts for almost 90% of agent removal.

The CF_3-CHF radical produced by (R3-1) is predicted to be removed primarily by two reactions, neither of which was included in the original HFC mechanism or in the kinetic model used in Ref. 8. Thermal dissociation to eliminate an F atom from the CF_3 group (R3–19) is the dominant removal mechanism. For this reaction we use the parameters from Ref. 9 with estimated falloff behavior. The HFC mechanism includes thermal decomposition reactions for fluorinated ethyl radicals involving C-H bond dissociation, but not C-F dissociation, the most likely process if the molecule contains a CF_3 group. It seems likely that analogous reactions should be added to the HFC mechanism for other fluoroethyl radicals. Reaction with H atom (R3-17) is predicted to be a secondary process in CF_3-CHF destruction. The reaction of CF_3-CHF with OH to produce CF_2CO, which Ref. 8 predicted to be the dominant removal reaction, is of minor importance under our conditions when (R3-17) and (R3-19) are considered.

The removal reactions of $CHF:CF_2$ are another area of the mechanism which appears to require attention. The inclusion of (R3-19) greatly increases the importance of this species in the kinetic pathways of HFP. When this reaction was added, predictions of flame speeds (discussed below) were greatly improved, but the concentration of CF_2 was overpredicted. The removal of $CHF:CF_2$ was predicted to almost exclusively by reaction (R1), which accounts for the overprediction of CF_2. This reaction is endothermic by about 10 kcal/mol.; the alternative product channel, CHF_2 + CHF, is too endothermic to be significant.

Reactions of $CHF:CF_2$ with O and OH are assumed in the HFC model to proceed by analogous pathways to those for ethylene [19],

$$CHF:CF_2 + O \Rightarrow CFO + CHF_2 \qquad (R2)$$

$$CHF:CF_2 + OH \Rightarrow CF_2:CF + H_2O. \qquad (R3)$$

It seems plausible that other channels may become more important as the ethylene becomes progressively more fluorinated. For the reaction of O atom with C_2F_4, the products are COF_2 + CF_2. We have postulated (R3-20) and (R3-21) as analogous product channels for the O atom reaction with trifluoroethylene. For the reaction of OH with ethylenes, H atom abstraction was the only product channel considered [19]. Reaction (R3) is essentially isothermic, and it appears that addition may be a more likely mechanism for OH attack on a heavily fluorinated ethylene. This possibility was not included in the HFC mechanism, partly because one possible set of products (following HF elimination) would be fluorinated vinoxy radicals, which are currently not included in the mechanism [19]. In (R3-22) and (R3-23) products are assumed to be a fluorinated methyl radical and a fluorocarbonyl (which could result from H atom migration followed by C-C bond rupture after the initial addition). This choice of products is motivated in part to avoid introduc-
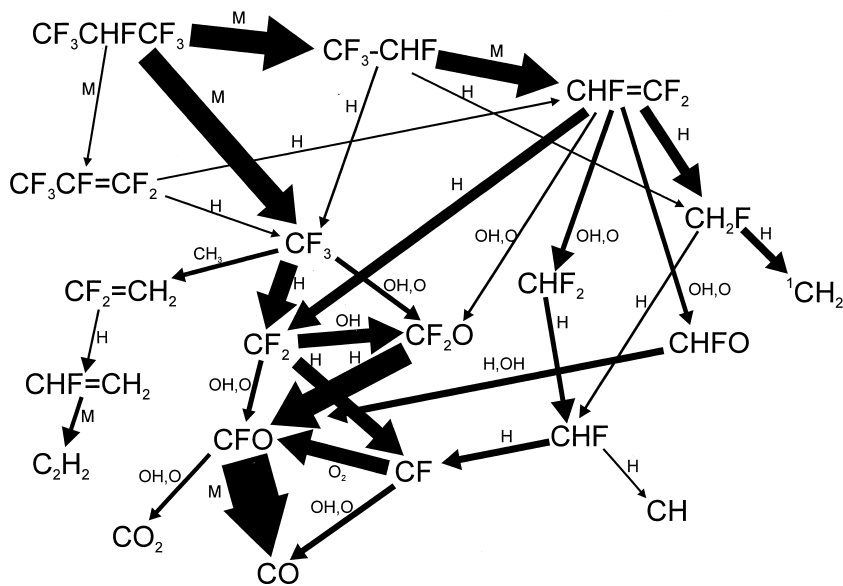
Fig. 9. Reaction pathways of fluorocarbon species in the $CH_4/O_2/C_3HF_7$ flame according to the kinetic mechanism. Arrow thicknesses are proportional to the molar flux of carbon-containing species. The most important reaction partner(s) are written next to each arrow in decreasing order of importance.

ing additional species into the mechanism. Both reactions are significantly exothermic.

Addition of (R3-20)–(R3-23) corrected the discrepancy in the CF_2 profile predictions caused by the addition of (R3-19). The flame profile data indicates that $CHF:CF_2$ reacts significantly with some species besides H, but it does not prove that the kinetics and products we have postulated are correct. In Ref. 19 it was remarked that consideration of additional product channels for the O and OH reactions with fluoroethylenes would be desirable at a subsequent stage of validation. We concur with this view in light of the importance of fluoroethylenes in the kinetic pathways of HFP and probably other fluoroethanes and fluoropropanes as well.

ATMOSPHERIC PRESSURE FLAME SPEED CALCULATIONS

Linteris et al. [12] published flame speed measurements of atmospheric pressure methane/air mixtures inhibited by HFP as well as other fluorinated ethanes and fluorinated propanes. Comparisons with calculations using the NIST HFC mechanism were reported for the fluorinated ethanes. No comparisons with model predictions were reported for HFP.

As an additional test of the HFP submecha-

nism, we performed flame speed calculations in comparison to the data of Linteris et al. [12]. Calculations were performed for flames containing mole fractions of approximately 3% HFP in methane/air mixtures with CH_4/O_2 ratios of 0.45, 0.50, and 0.55. The flame speed calculations were performed on a domain extending 25 cm from the flame on the cold boundary, and 60 cm on the hot boundary. The calculations used multicomponent viscosities, thermal diffusion for H and H_2, and windward differencing on the convective term. The initial temperature of the fresh gases was set to 298.2 K. The solutions were obtained on meshes having 150 grid points. Previously, we used the same kinetic mechanism employed here (without the HFP submechanism) to calculate flame speeds of $CH_4/air/CHF_3$ and $CH_4/air/CH_2F_2$ mixtures [7]; good agreement with experimental data was obtained for all conditions except for difluoromethane-inhibited flames at high equivalence ratios ($\phi > 1.25$).

In initial calculations, predicted flame speeds in the three HFP-inhibited mixtures were far too low, ranging from 40% to 70% of the experimental values. Sensitivity and reaction pathway analysis indicated that thermal decomposition should dominate HFP removal, and that predominance of C-C bond dissociation as opposed to HF elimination should increase

TABLE 4

Calculated Flame Speeds of CH_4/air/CF_3CHFCF_3 Mixtures

CH_4/O_2 ratio	HFP mole %	Calculation		Experiment[b]		$(U/U_o)_{calc}/(U/U_o)_{exp}$
		U (cm/s)	U/U_o[a]	U	U/U_o	
0.45	2.96	17.76	0.50	22.8	0.61	0.83
0.50	2.93	16.27	0.41	15.4	0.37	1.11
0.55	2.91	12.32	0.31	17.4	0.44	0.70

[a]Speed normalized by speed of uninhibited CH_4/air flame at same CH_4/O_2 ratio.
[b]Ref. 12.

flame speed. This effect is presumably due to the creation of two radicals by (R3-1), as opposed to two stable species by (R3-2). In Ref. 9 Hynes et al. derived new rate expressions for the HFP decomposition reactions, and added (R3-19) for CF_3-CHF removal. The revised kinetic parameters for (R3-1) and (R3-2) greatly increased the predicted predominance of C-C bond rupture in HFP removal, and led to flame speed predictions 1–2 cm/s higher.

The addition of (R3-19) caused a much larger increase in the predicted flame speed for all stoichiometries. The F atom generated by this reaction reacts predominantly with water to yield HF + OH, generating one of the important flame radicals. Addition of Reactions (R3-20)–(R3-23) did not significantly affect the predicted flame speed. Using the final mechanism as detailed in Table 1, the calculated flame speed results are given in Table 4. The predictions agree with the experimental data within 30% for all three test cases. The prediction is least accurate for the rich stoichiometry, where formation of larger HFC species not included in the present mechanism is most likely to be most important.

One unusual aspect of the experimental flame speed measurements reported by Linteris et al. was that at a fixed agent concentration, HFP caused a greater reduction in flame speed for the 0.50 methane/oxygen ratio than for the 0.55 ratio. By contrast, all other HFCs agent tested caused a progressively greater reduction in burning velocity as the methane/oxygen ratio was increased between 0.45 and 0.55. Our calculation does not predict the behavior observed experimentally for HFP; rather, it predicts that the inhibition effectiveness becomes progressively greater as the stoichiometry becomes richer.

It is noteworthy that in Ref. 12, burning velocities were significantly underpredicted for mixtures inhibited by CF_3-CH_2F and CF_3-CHF_2. CF_3-CH_2F is largely converted to CF_3-CHF by hydrogen abstraction, while CF_3-CHF_2 forms CF_3-CF_2. Based on the current modeling results for HFP, the addition of Reaction (R3-19) and an analogous decomposition for CF_3-CF_2 should significantly increase the predicted flame speeds from the values obtained in Ref. 12, improving agreement with the experimental measurements.

DISCUSSION

The agreement between the experimental intermediate species data and the predictions of the kinetic model is quite good. There is a slight discrepancy in the predictions of CF_2 profiles, suggesting that removal kinetics of fluorinated ethylenes by O and OH require further investigation. The addition of Reactions (R3-20)–(R3-23) was the only change made to the mechanism on the basis of improving the fit to the experimental profiles. No changes whatsoever were made to the C_1 fluorocarbon kinetics, because predictions of fluoromethane-inhibited flame structures are sensitive to these reactions, and any alterations would have to be validated against the data modeled in Ref. 7.

The kinetics of the HFP and CF_3-CHF thermal decomposition reactions given in Ref. 9 greatly improve predictions of burning velocities; we have adopted these rate expressions for this reason. In Ref. 9 additional reactions and species were included in the kinetic mechanism which were not included in Ref. 8. We have not incorporated these into our mechanism since they are likely to be less important in a near-

stoichiometric flame than in a purely pyrolytic environment. It is possible, however, that for rich stoichiometries or higher inhibitor concentrations these may need to be considered. The C_3 reaction set used here is minimal in size compared to the C_2 reactions in the NIST HFC mechanism and it should not be considered as being comprehensive.

To investigate the applicability of the mechanism given here to the conditions of Hynes et al., we modeled the conditions of Ref. 10 using the experimental temperature profile as input. The model calculations of species profiles were qualitatively similar to those obtained by Hynes et al. There were some differences; in particular the COF_2 concentration was calculated to be about 30% higher as a result of our modifications to the C_1 kinetics in Ref. 7. Hynes et al. measured somewhat lower concentrations of this species in the postflame zone than were predicted by their mechanism. Secondary reactions (hydrolysis in particular) of COF_2 following probe sampling may, however, account for the discrepancy [8]. The differences in the mechanisms between that used here and that of Ref. 10 had a much smaller effect on the species profiles than did the perturbations introduced by the sampling probe, which Hynes et al. treated phenomenologically. The experimental data presented in [10] does not appear to unequivocally favor either mechanism over the other.

The agreement of the modeling predictions using the current mechanism with the species profiles is very encouraging since there are significant differences in stoichiometry, pressure, and temperature between the present experiment and the conditions studied by Hynes et al. The present data set is only an indirect measure of the initial HFP decomposition pathways, since all the species monitored are several reactions removed from the original agent. Other sets of validation data are desirable to experimentally verify the kinetic pathways of HFP in flames.

In terms of refinements to the HFC mechanism, it appears that thermal decomposition reactions of fluoroethyls to produce atomic fluorine are important and need to be added. This is likely to have implications for modeling inhibition by C_2 as well as C_3 agents. Revision of O and OH reaction kinetics with fluoroethylenes will impact flame structure calculations, but appears to have little effect on global parameters such as flame speed.

REFERENCES

1. Miziolek, A. W., and Tsang, W., Eds., *Halon Replacements: Technology and Science*, ACS Symposium Series 611, American Chemical Society, Washington, DC, 1994.

2. Sheinson, R. S., Penner-Hahn, J. E., and Indritz, D., *Fire Safety J.* 15:437–450 (1989).

3. Nyden, M. R., Linteris, G. T., Burgess, Jr., D. R. F., Westmoreland, P. R., Tsang, W., and Zachariah, M. R., in *Evaluation of Alternative In-Flight Fire Suppressants for Full-Scale Testing in Simulated Aircraft Engine Nacelles and Dry Bays* (W. L. Grosshandler, R. G. Gann, and W. M. Pitts, Eds.), NIST SP 861, 1994, pp. 467–642.

4. Westmoreland, P. R., Burgess, Jr., D. R. F., Zachariah, M. R., and Tsang, W., *Twenty-Fifth Symposium (International) on Combustion*, The Combustion Institute, Pittsburgh, 1994, pp. 1505–1511.

5. Burgess, Jr., D. R. F., Zachariah, M. R., Tsang, W., and Westmoreland, P. R., *Prog. Energy Combust. Sci*. 21:453 (1996).

6. The current NIST HFC mechanism may be downloaded from http://fluid.nist.gov/ ckmech.html.

7. L'Espérance, D., Williams, B. A., and Fleming, J. W., *Combust. Flame* 117:709–731 (1999).

8. Hynes, R. G., Mackie, J. C., and Masri, A. R., *Combust. Flame* 113:554–565 (1998).

9. Hynes, R. G., Mackie, J. C., and Masri, A. R., *J. Phys. Chem. A* 103:54–61 (1999).

10. Hynes, R. G., Mackie, J. C., and Masri, A. R., *Energ. Fuel* 13:485–492 (1999).

11. Westbrook, C. K., *Combust. Sci. Technol.* 34:201 (1983).

12. Linteris, G. T., Burgess, Jr., D. R., Babushok, V., Zachariah, M., Tsang, W., and Westmoreland, P., *Combust. Flame* 113:164–180 (1998).

13. L'Espérance, D., Williams, B. A., and Fleming, J. W., *Chem. Phys. Lett.* 280:113–118 (1997).

14. Kee, R. J., Grcar, J. F., Smooke, M. D., and Miller, J. A., PREMIX: A Fortran Program for Modeling Steady Laminar One-Dimensional Premixed Flames, Sandia Report SAND85-8240, 1985.

15. Kee, R. J., Rupley, F. M., and Miller, J. A., Chemkin-II: A Fortran Chemical Kinetics Package for the Analysis of Gas-Phase Chemical Kinetics, Sandia Report SAND89-8009, 1989.

16. Kee, R. J., Warnatz, J., and Miller, J. A., A Fortran Computer Code Package for the Evaluation of Gas-Phase, Multicomponent Transport Properties, Sandia Report SAND83-8209, 1983.

17. Bowman, C. T., Hanson, R. K., Gardiner, W. C., Lissianski, V., Frenklach, M., Goldenberg, M., and Smith, G. P., *GRI-Mech 2.11—An Optimized Detailed Chemical Reaction Mechanism for Methane Combustion and NO Formation and Reburning,* GRI Report GRI-97/0020, 1997, Gas Research Institute, Chicago. http://www.ME.Berkeley.edu/gri−mech/

18. Hynes, R., private communication.

19. Burgess Jr., D. R. F., Zachariah, M. R., Tsang, W., and Westmoreland, P. R., *Thermochemical and Chemical Kinetic Data for Fluorinated Hydrocarbons*, NIST Technical Note 1412 (1995).